Sansoni: 3D Optical Whole-Field Range Sensor: Procedures for Automatic Set-Up of Measurement & Calibration

Wednesday, February 10, 2021 4:20 PM

00777038

3D Optical Whole-Field Range Sensor: Development of Procedures for the Automatic Set-Up of the Measurement and the Calibration of the System

Giovanna Sansoni
INFM and Lab. of Optoelectronics, Dept. of Electronics for the Automation
University of Brescia
Via Branze 38, I-25123 Brescia - Italy

Abstract

In this paper, the procedures developed to enhance the flexibility and the robustness of an optical whole-field profilometer are presented, as well as the procedure for calibrating it. The system is based on active triangulation. In order to comply with a sufficiently wide typology of targets, three different techniques to perform light coding have been integrated. In order to guarantee a sufficient robustness and simplicity of use, the system has been equipped with a procedure for the automatic determination of the measurement parameters, both geometrical and optical. Good linearity has been observed, and an overall mean value of the measurement error equal to 40 μm, with a variability of about ±35 μm, corresponding to 0.06% of full scale have been estimated.

1. Introduction

3-D imaging sensors are becoming increasingly relevant in a wide range of applications. In the industrial field, for example, optical range sensors can play a key role in the production quality control, as well as in rapid prototyping and reverse engineering applications, due to the intrinsic non contact nature of the measurement, and to the possibility of markedly shortening the measurement time [1].

Many techniques have been developed, both passive and active [2]. In the active approach, both scanning systems, using coherent light sources, and whole field profilometers, based on incoherent light projection have been developed.

A whole field profilometer has been developed at our laboratory, based on active triangulation [3]. A Liquid Crystal projector projects suitable patterns of structured light on the target, these patterns are acquired by a video camera and elaborated in order to obtain the range information. The triangulation is based on the evaluation of the shift that the light directions from the projector undergo due to the presence of the object under measurement with respect to their position on a flat surface, taken as a reference for the measurement.

The univocal description of the light directions is achieved by suitable light coding. In order to comply with a sufficiently wide variability of the target shape, three different methods have been developed so far. The first one is based on the gray code method (GCM), the second one on the phase shift method (PSM), and the third one on a suitable combination of GCM with PSM (GCPS) .

The integration of different light codings markedly increases the flexibility of the system, as well as its complexity, as to the measurement set-up, and the calibration of the system.

The set-up phase is not trivial, especially in view of using the system in the industrial production field. In fact, given a target for the measurement, the processes of (i) choosing the suitable coding procedure, (ii) determining the correct geometrical set-up, and (iii) selecting the proper approach for the triangulation, should be performed automatically.

In the system, all these tasks are carried out by a suitably designed procedure, aimed at determining the proper coding method in dependence of the required resolution and at setting the values for the geometrical parameters of the system. These information is then used to correctly perform the triangulation.

As part of the work performed, we analyzed the systematic measuring errors, depending mainly on the geometry of the projector and vision devices. The results of this study allowed us to develop a suitable calibration procedure, determining the estimates of the parameters of the measurement at optimal accuracy and speed.

In this paper, the procedures for the automatic set-up of the measurement and for calibrating the system are presented in detail, and a number of experimental results are reported.

0-7803-5276-9/99/$10.00 © 1999 IEEE

2. Coding techniques and triangulation

Fig. 1 shows the layout of the system. An LCD-based unit projects light patterns along a direction at an angle α with respect to that of acquisition. Points C and P represent the entrance and exit pupils of the video camera and of the projector respectively. The optical geometry is modeled by means of three parameters: these are the distance between points C and P, called baseline d, the distance L of the baseline from a reference surface R, and the orientation of the projector with respect to the video-camera, expressed by angle α. It is assumed that both baseline d and the image plane are parallel to reference R and that the optical axis of the video camera forms with the optical axis of the projector a plane perpendicular to plane R. FW is the width of the field of view along the x-coordinate. The images are acquired with resolution of 800x2621 (NxM) pixels, and the gray level range is 256.

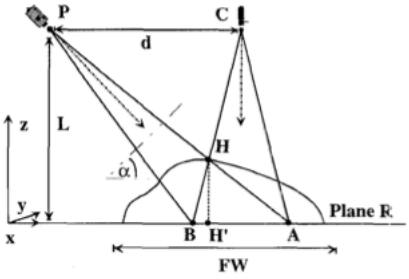

Fig. 1. Optical geometry of the system

The triangulation formula is obtained by observing that the direction of projection $\overline{PA}$ is seen by the video camera at point A on plane R when the object is absent, and at point B when the object is present. The height $Z_H(x,y)=\overline{HH'}$ of the object at point H(x,y) can be evaluated by observing that triangles BHA and PHC are similar, and that the following triangulation equation holds:

$$Z_H(x,y)=\frac{L\cdot S_R(x,y)}{d+S_R(x,y)} \qquad (1)$$

In Eq. (1), $S_R(x,y)$ equals segment $\overline{AB}$ on plane R, and represents the shift that the direction of projection $\overline{PA}$ undergoes due to the object height at point H(x,y). Thus, a preliminary step to the use of Eq. (1), is the evaluation of parameter $S_R(x,y)$. This step is performed by suitable light projection and coding.

2.1. Evaluation of $S_R(x,y)$ by means of GCM

GCM is based on the projection in n subsequent steps, of n fringe patterns, which define in the working space 2^n directions of projection, univocally described by the words of a n-bit gray code. These patterns are acquired and binarized, and stored into a matrix, defined onto the CCD, called Bit Plane Stack (BPS). Each element (j,k) of BPS stores a code word which is then mapped to an integer number, denoted as $\hat{1}$, by using a proper look-up table. The same sequence of patterns is projected in the absence and in the presence of the object: two matrixes are obtained for the reference and for the object, respectively called BPS_R and BPS_O. Shift $S_R(x,y)$ is evaluated by means of:

$$S_R(x,y)=(j^*-j)\cdot\frac{FW}{N} \qquad (2)$$

Eq.(2) highlights that $S_R(x,y)$ is computed at the image plane by searching, for each element (j,k) in BPS_R, the position (j*,k) in BPS_O, where equal code number $\hat{1}$ is stored.

The univocal correspondence between the directions of projection and their codings allows the measurement of objects characterized by shape discontinuities. The binarization of the measurement area results in high repeatability; on the other hand, the resolution is rather low, due to the fact that in Eq. (2) term (j^*-j) is an integer [4].

2.2. Evaluation of $S_R(x,y)$ by means of PSM

PSM follows the well known approach based on the projection of n_p periodic patterns with spatial period p; each pattern is obtained by spatially shifting the preceding one of a fraction p/n_p of the period. The intensity fields $I_i(j,k)$ acquired in correspondence with each shift (i=0, 1, 2, 3 for n_p=4) are elaborated in order to determine the phase information which codifies the light directions. It can be demonstrated that the following equation holds [5]:

$$\Phi(j,k)=\tan^{-1}\frac{I_1(j,k)-I_3(j,k)}{I_0(j,k)-I_2(j,k)} \qquad (3)$$

Two phase matrices are obtained, for the reference and for the object, respectively called $\Phi_{Ref}(j,k)$ and $\Phi_{Obj}(j,k)$, and shift $S_R(x,y)$ is evaluated at the projector LCD plane by means of the following relationship:

$$S_R(x,y)=\frac{p_R}{2\pi}\left[\Phi_{Obj}(j,k)-\Phi_{Ref}(j,k)\right] \qquad (4)$$

where p_R is the period of the fringes at reference R. The ambiguity of the phase makes this method suitable for the measurement of smooth objects; on the other hand, phase values are continuously distributed on the scene, and the resolution of the measurement is high.

2.3. Evaluation of $S_R(x,y)$ by means of GCPS

GCPS can be viewed as a cascade of GCM and PSM: the last pattern of the GCM sequence is omitted, the least significant bit of the resulting, incomplete coding is computed by means of PSM, and the complete coding of the light directions is real number l(j,k) obtained as follows:

$$l(j,k) = \hat{l}(j,k) + \frac{2}{\pi}\left[\Phi(j,k) + \Delta\Phi(j,k)\right] \quad (5)$$

In Eq.(5), $\hat{l}(j,k)$ is the integer coding obtained by the projection of the gray code sequence, $\Phi(j,k)$ is the phase value evaluated by the phase shift approach, and $\Delta\Phi(j,k)$ represents a phase correction term, experimentally evaluated.

In GCPS, shift $S_R(x,y)$ is evaluated directly at reference plane R, by mapping the light codings into the corresponding abscissas along the x- coordinate. This means, for the example in Fig. 1, that abscissas x_A and x_B of points A and B along x- are firstly evaluated, and then shift $S_R(x,y)$ is computed as:

$$S_R(x,y) = \left[x_A - x_B\right] \quad (6)$$

The transformation of light codings l(j,k) into abscissas is performed by a suitable mapping, which accounts for the mutual orientation of the projector and of the video-camera, expressed by angle α. For example, denoting with $l_{(PB)}$ the coding of ray $\overline{PB}$, the corresponding abscissa x_B is obtained by means of the following trigonometric relationships:

$$X_B = L \cdot \left(\tan\left(\gamma - \operatorname{atan}\left(\frac{C_l \cdot lp_{(PB)} \cdot \cos(\gamma - \alpha)}{1 + C_l \cdot lp_{(PB)} \cdot \sin(\gamma - \alpha)} \right) \right) \right) \quad (7)$$

The analytical derivation of Eq. (7) is out of the scope of this paper. The interested reader is addressed to the publication [5]. Here it is worth noting that C_l is a constant, expressed as:

$$C_l = \frac{\sin(\delta_{tot})}{nlp \cdot \sin(\theta_{tot})} \quad (8)$$

where parameter nlp represents the total number of light codings that fall within the field of view at plane R, and angles δ_{tot}, θ_{tot} and γ are functions of α. Eq.(7) models the nonlinear dependence of the abscissa x_B of point B on either light coding $lp_{(PB)}$, and parameters L and α. A linear mapping, such as in Eqs.(2) and (4) can not be successfully applied in GCPS. In fact, Eq.(2) specifically requires that the light codings are integer numbers $\hat{l}$, while Eq.(4) can be used only if period p_R can be considered constant on reference R. However, this hypothesis is not valid, due (i) to the crossed-optical-axes geometry of the system (points P and C are not at infinity) and (ii) to the geometrical setups typical of GCPS, characterized by smaller values for L and larger values for d with respect to PSM: these two characteristics determine a non negligible variation of period p_R with x-, even on plane R. Thus, any attempt to evaluate shift $S_R(x,y)$ by means of Eq.(4) inherently yields an error in the estimation of the height. In [5], it has been demonstrated that this error is particular evident on flat surfaces: the measured profile reveals a slope increasing with both x- and z-. However, the entity of this error is very often negligible when PSM is used, while it must be compensated for in GCPS. The use of Eq. (7) performs this compensation, because it precisely models the relationship between the position along x- of the points where the projected light rays intersect reference R and the corresponding light codings. This derivation is performed punctually, and is intrinsically insensitive to any variation of p_R.

GCPS reveals to be very powerful when both extended measuring range and high resolution are required, as in the case of objects presenting steep slope changes and fine surface details.

3. Procedure for the system set-up

The good performance in terms of resolution achievable by means of PSM results into values for distance L up to 5 m, and for ratio L/d, typically in the range 3.5-5. In contrast, in GCM, the low height resolution limits the dimension of the field of view, and reduces distance L to values close to 1 m and the ratio L/d to values close to 1. The same situation holds even for GCPS, which shares the same geometry as GCM. The procedure for the set-up of the measurement automatically selects the proper light coding method, and correspondingly determines the optimal values for L and d. It receives as inputs (i) the required height resolution z_{min}, (ii) the dimensions X, Y, Z of the measuring volume, and (iii) a concise description of the object topography. The knowledge of the topography of the object allows the procedure to make a first choice about the coding technique. Then starting from values X and Y, a simple iterative algorithm sets the initial values for

distance L and the field of view in order to frame the whole object. The focal length f is set in order to guarantee that the focus condition holds on plane R and along the measuring range. The last parameter to be determined is the baseline distance d. If the measurement procedure is GCM, d is evaluated as [4]:

$$d = \frac{FW}{N} \cdot \frac{L}{z_{min}} \tag{9}$$

If ratio L/d is close to 1 the procedure stops: in fact, in this case GCM shows optimal performance. If this condition is not satisfied, GCPS is chosen, and d is evaluated by substituting Eq. (4) into Eq. (1):

$$z_{min} = \frac{Lp\Phi_{min}}{2\pi d + p\Phi_{min}} \tag{10}$$

In Eq.(10), p is the mean value of the spatial period of the finest fringe pattern used in GCPS, and Φ_{min} is the minimum phase value that can be obtained. In our system, this value is set to about three times the phase value theoretically evaluated by taking into account only for the quantization error of the gray levels. Eq. (10) is then solved with respect to parameter d:

$$d = \frac{Lp\Phi_{min} - p\Phi_{min}z_{min}}{2\pi z_{min}} \tag{11}$$

The exit condition is the same as in GCM. If it is not verified, the procedure sets d=L (this choice generally allows us to obtain good performance) and calculates the achievable resolution z^*_{min} by means of Eq. (10).

Eqs. (10) and (11) are used also when the initial choice for coding is PSM; if ratio L/d is in the range typical of phase coding, the exit condition is matched, otherwise d is set equal to L/4, and the resolution z^*_{min} is set as output.

4. Calibration of the system

The calibration has been specifically designed to comply with GCPS; however, it can be used in GCM and PSM as well, without any variation. The basic criterion to calibrate the system is exemplified in Fig. 2, where the error on the measured height due to coarse estimates of parameters α, L and d in Eqs. (7) and (1) is shown. The target is a block of parallepipedic shape and height equal to 60 mm ± 0.01 mm. The initial estimates for α, L and d are α_0= 0.455 rad, L_0=1192 mm and d_0=583 mm. The 3D profile of the object measured along a section parallel to x- is plotted in the height range from 50 to 70 mm (bold, dashed line). The measured height dramatically depend on x-: the linear regression on the data shows an angular coefficient m_0=0.012, and results into a difference in level along the z- coordinate equal to 2.38 mm, corresponding to 3% of the nominal height.

The reduction of angle α to α_1=0.321 rad strongly reduces this dependence (light, solid line): the regression line is now characterized by angular coefficient m_1=0.0001. The difference in level along z- is 0.02 mm; however, mean value ΔZ of the difference between the measured heights and the nominal one is still high, and results ΔZ=3.57 mm. By varying L and d respectively to L_1=1135.35 mm, and d_1=573 mm, the measured profile shows better accuracy (dark, solid line): the intercept of the regression line is 59.58 mm, and ΔZ is now equal to 0.02 mm.

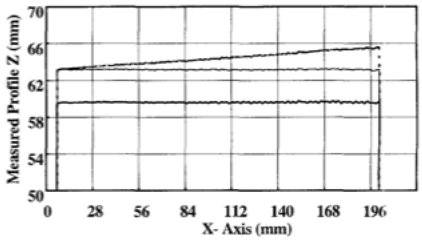

Figure 2. Influence of parameters α, L and d on the measured 3D profile.

The calibration procedure exploits the dependence of the measured height on the system parameters above described: it determines for angle α the estimate α_c which minimizes the slope of the profile, and evaluates for L the estimate L_c which minimizes ΔZ. Parameter d is evaluated to the required accuracy during the set-up of the system, and is not involved into the calibration: this choice allows strong simplification of the procedure and does not reduce its performance: in fact, in Eq. (1), L and d are independent parameters and, in principle, the same value as before for ΔZ can be obtained by finely varying L while leaving d unchanged.

The calibration master is a block of parallepipedic shape; its nominal height, measured by a CMM with uncertainty one magnitude order better than that one foreseen for our sensor, is Z_{nom}=80 mm±0.01 mm. The algorithm starts from the initial, rough estimates of L and α, denoted by L_0 and α_0 and is composed of two nested loops: the outer one, indexed by parameter n, evaluates L_c, the inner one, indexed by parameter i, determines α_c.

At each iteration n of the outer loop, the procedure calculates $[Z]^A_n$, which represents the profile of the master measured in correspondence with section A, parallel to x-, at half of the illuminated area. The exit condition is that the mean profile measured on the master is within a

predefined tolerance δZ with respect to the nominal height. Denoting with $\overline{\Delta Z}$ the mean value of error $\Delta Z = [Z]_n^A - Z_{nom}$, this condition is expressed as $|\overline{\Delta Z}| < \delta Z$. If $|\overline{\Delta Z}| > \delta Z$, the regression line is evaluated over $[Z]_n^A$ and both angular coefficient m_n and intercept q_n are determined. If $|m_n| < \delta m$, current value α_i for angle α does not need any variation, and the procedure calculates a finer estimate L_{n+1} of L. This is accomplished by exploiting the linear dependence of the height on L in Eq.(1). Value L_{n+1} is then used to determine vector $[Z]_n^A$ at the next iteration of the outer loop. If the exit condition is verified, current values L_n and α_i are assigned to the searched estimates L_c and α_c and the calibration stops; otherwise it enters the next iteration.

If $|m_n| > \delta m$, the procedure enters the inner loop. The exit condition of the inner loop is that the slope of the master profile is within a predefined tolerance δm. The slope is expressed by angular coefficient m_i of the regression line evaluated over the profile $[Z]_i^A$ measured by the sensor, thus, the exit condition is $|m_i| < \delta m$. At each iteration i, a new value α_{i+1} is evaluated as $\alpha_{i+1} = (1 + w \cdot m_i) \cdot \alpha_i$, where w is a weight factor, experimentally determined. Then, α_{i+1} is assigned to current value α_i, and angular coefficient m_i and intercept q_i of the regression line evaluated over vector $[Z]_i^A$ are correspondingly determined. If $|m_i| < \delta m$, the procedure leaves this loop and returns to the outer one, for parameter L.

This algorithm can be equally applied even to GCM and to PSM. In GCM, vector $[Z]_n^A$ depends only on parameters L and d, through Eqs. (2) and (1). Actually, Eq. (2) makes the measurement intrinsically insensitive to any variation of period p_R, thus, the condition $|m_n| < \delta m$ is always verified, the procedure never enters into the inner loop, and only parameter L_c is evaluated and used in Eq. (1). In PSM, vector $[Z]_n^A$ depends only on parameters L and d, through Eqs. (4) and (1). In principle, use of Eq.(4) introduces the dependence of the measurement on the variation of period p_R; however, the values for L and d chosen by the procedure for the automatic set-up of the system make this influence very small. Consequently, the condition $|m_n| < \delta m$ is very often verified, and only parameter L_c is determined. However, if the procedure enters the inner loop, the evaluation of shift $S_R(x,y)$ is performed automatically by Eqs. (7) and (6), both L_c and α_c are evaluated as for GCPS, and the influence of any variation of p_R is intrinsically compensated for.

5. Experimental results

An extensive set of measurements has been performed to test the effectiveness of the calibration procedure and to evaluate the overall performances of the system. The Input-Output characteristic curve of the system has been evaluated. The target is a plane 300 x 50 mm (length x width), with height equal to 4 mm ± 0.01 mm, mounted on a translation stage to explore a range along Z- equal to 80 mm, at steps of 4 mm each. In the following, the input height values are denoted by Z_{in}, (Z_{in}=4, 8,...,80 mm). At each position Z_{in} the measurements are repeated 30 times. Fig. 3 shows the In-Out characteristic curves of the calibrated system, as a function of both Z_{in} and x-. The coefficient R of the regression lines evaluated over each curve is R=0.9999. It is well evident from this figure that the dependence on x- is canceled out by the calibration, as both the slope and the offset of the profiles measured along x- are kept within small tolerances, even at heights Z_{in} markedly far from the value Z_{nom}=80 mm for which L_c and α_c have been derived. The linearity error evaluated over each curve shows a maximum value lower than 50 µm, and a variability of 25 µm. The dependence of the measurement error vs. Z_{in} is considered in Fig. 4, which plots both the mean value and the variability of the measurement error Δz along a section parallel to the x-coordinate, as a function of Z_{in}. This figure well demonstrates the ability of the calibration to bound the measurement error within a range of 12-33 µm, with a variability of ±37 µm.

Finally, the measurement of a ceiling light and of a bass-relief (shown in Fig. 5) is reported. GCPS has been used, parameters L and d have been determined in the set-up phase (L/d=0.9), and values L_c and α_c by the calibration procedure. The 3D profiles are shown in Figs. 6 and 7: the standard deviation evaluated over a set of 50 measurement is equal to 40 µm.

6. Conclusions

In this paper, the main features of an optical whole field profilometer based on the projection of structured light have been presented. The flexibility of the system has been optimized by integrating different approaches to

the coding of light directions as well as suitable mapping procedures to perform the triangulation. A specifically developed procedure for the measurement setup guarantees the robustness and the effective usability of the system in the industrial measurement practice. The calibration procedure is also presented: it is simple, robust, and performs at optimal speed.

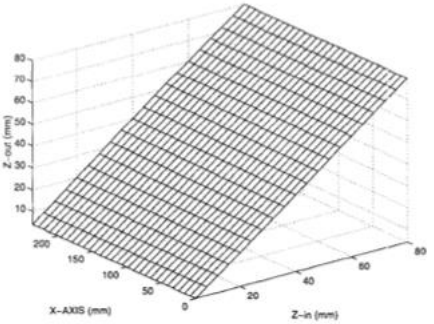

Fig. 3. In-Out characteristic curve of the system.

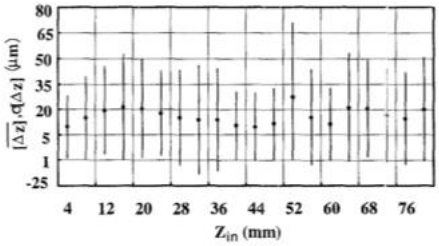

Fig. 4. Evaluation of the accuracy of the system.

7. References

[1] P. Boulanger, "Reverse Engineering of Complex Surfaces based on a New Hierarchical Segmentation Method," *Proc. of SPIE, Videometrics II*, Vol. 2097, 186-197, 1993.

[2] R.A. Jarvis, "A perspective on range finding techniques for computer vision," *IEEE Trans. Pattern Anal. Mach. Intel.*, Vol. 5, No. 2, 122-139, 1983.

[3] G. Sansoni, M. Carocci, S. Lazzari, R. Rodella, "A 3D imaging system for industrial applications with improved flexibility and robustness," *J. Opt. A:Pure Appl. Opt.*, No. 1, 1-11, 1999.

[4] G. Sansoni, S. Corini, S. Lazzari, R. Rodella, and F. Docchio, "3-D Imaging based on Gray code light projection: characterization of the measuring algorithm and development of a measuring system for industrial applications," *Appl. Opt.*, Vol. 36, No. 19, 4463-4472, 1997.

[5] G. Sansoni, S. Lazzari, S. Peli, and F. Docchio, "3D Imager for dimensional gauging of industrial workpieces: state of the art of the development of a robust and versatile system," *Proc. of Intern. Conf. on Recent Advances in 3-D Digital and Modeling*, 19-26, 1997.

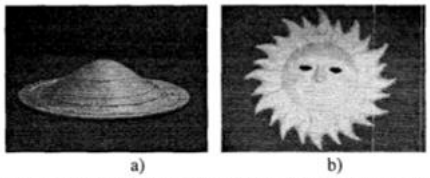

a) b)

Fig. 5. Test objects. 5.a): ceiling light; 5.b): bass-relief.

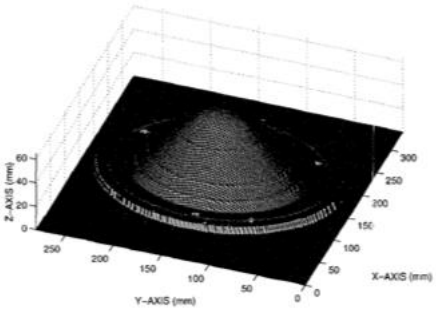

Fig. 6. Whole 3D profile of the ceiling light.

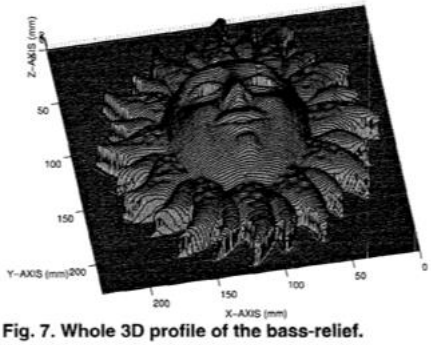

Fig. 7. Whole 3D profile of the bass-relief.